SERS Detection of Charge Transfer at Electrochemical Interfaces using Surface-bound Ferrocene

Ruoxi Li³, Imran Chaudhry⁵, Cindy Tseng², Yu Wang⁴, Bofan Zhao³, Indu Aravind¹, Sizhe Weng³, Zhi Cai⁴, Jahan Dawlaty², Lasse Jensen⁵, and Stephen B. Cronin^{1, 2, 3}

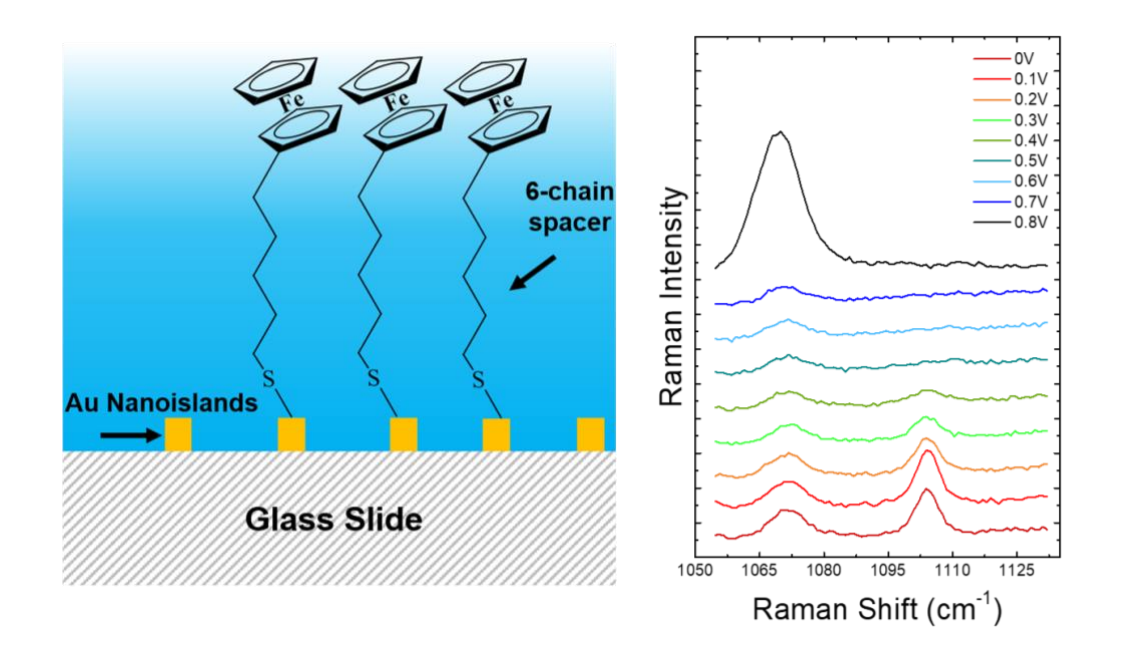
¹Department of Physics and Astronomy, ²Department of Chemistry, ³Ming Hsieh Department of Electrical Engineering, ⁴Mork Family Department of Chemical Engineering and Materials Science, University of Southern California, Los Angeles, CA 90089, USA

⁵Department of Chemistry, Pennsylvania State University, University Park, PA 16802, USA

Abstract: We present the novel use of surface enhanced Raman scattering (SERS) spectroscopy to detect charge transfer in ferrocene/ferrocenium (Fc/Fc⁺) bound to an active electrode under electrochemical working conditions. The ferrocene has a 6-carbon linker with a thiol tether (6-(ferrocenyl)hexanethiol) and produces Fc/Fc⁺ couple voltammograms exhibiting charge transfer above 0.4V vs. Ag/AgCl. By observing *in situ* micro-Raman spectroscopy with a water immersion lens, we observe significant changes in the spectra that corresponds to the charge state oxidation to ferrocenium (Fc⁺). In particular, the Fc⁺ state is characterized by the disappearance of the C_p-breathing mode (1104cm⁻¹ peak) and an 11-fold increase in the hexanethiol tail mode around 1072cm⁻¹. Raman spectra calculated by density functional theory exhibit predominant peaks that agree well with our experimental observations and indicate that the Fc \rightarrow Fc⁺ transition is associated with a change in the orientation, which gives rise to dramatic changes in the Raman spectra.

Keywords: Local electric field, in-situ Raman, monolayer graphene, operando, catalysis, plasmonic

TOC Figure



Charge transfer at electrode/electrolyte interfaces is a critical step in nearly all electrocatalytic and photocatalytic processes. Much progress has been made in recent years understanding the mechanisms and kinetics of electrocatalytic and photocatalytic systems. However, the precise potential at which charge transfer occurs is often elusive. For semiconductor photoelectrodes, the surface potential is complicated by band bending and quasi-Femi level splitting at the semiconductor surface. Therefore, having a surface-bound molecule with a well-defined redox potential whose charge state can be monitored spectroscopically, is of great interest. These so-called "charge transfer reporters" have been demonstrated using transient absorption spectroscopy but not Raman spectroscopy. Facile spectroscopic tools for studying these charge transfer events are lacking.

Over the past few years, electrochemical surface enhanced Raman spectroscopy (EC-SERS) has been used as a common analytical tool. However, a vast majority of these prior studies focus on sensing/detection of harmful molecules and biological species. 1-5 EC-SERS work in the area of electrochemical cleaning enables sensors/detectors to be reused multiple times. 6-7 EC-SERS has been used to monitor electrodeposition *in situ*. 8-9 Several EC-SERS studies have also been published on dye molecules, including nile blue (NB) and rhodamine 6G (R6G), in aqueous and non-aqueous environments. 10-11 Spectral shifts were attributed to electrochemical charge transfer, although no detailed calculations were performed to corroborate these findings. The use of EC-SERS in conjunction with specific surface reporter molecules tethered to an electrode surface for detecting charge transfer and surface potential spectroscopically present a viable path towards obtaing a better understanding of electrochemical and photoelectrochemical processes, however, such studies have not been carried out in the existing literature.

Ferrocene has been studied extensively, with more than 20,000 publications as of this writing. The use of ferrocene to study charge transfer at electrode interfaces dates back the early 1980s. 12 As a well-defined redox couple (i.e., Fc/Fc⁺), cyclic voltammetry (CV) has been used to study charge transfer at electrode surfaces.¹³ Paul et al. studied the tunable redox potential and optical properties of modified ferrocene-based complexes, which span a range from +0.4 V down to -0.1 V versus SCE.¹⁴ Smalley et al. studied the kinetics of electron transfer of ferrocene-terminated alkanethiol monolayers on gold as a function of number of methylenes in the alkyl chain tethering on gold. 15 Choudhury, et al. have functionalized semiconductor surfaces with ferrocene in order to study photoexcited charge transfer.¹⁶ Swearingen et al. reported absorption spectra showing dramatic changes in the visible range upon oxidation of ferrocene to ferrocenium, with a shift in peak absorption from ferrocene at 445 nm to ferrocenium at 619 nm. 17 Previous studies using surface-enhanced infrared absorption spectroscopy (SEIRAS) have examined Fc-terminated electrode systems as a function of electrode potential.²⁰⁻²¹ While these spectra lend some insight into the changes observed in the present study, it should be noted that the spectral resolution of the SEIRAS approach is at least one order of magnitude lower than that of Raman spectroscopy and, as such, approach is unable to distinguish the 2 peaks reported here (1072 and 1104 cm⁻¹).

In the work presented here, SERS active electrodes are fabricated by depositing 5nm of Au on a glass slide using electron beam deposition. These thin films of Au are not thick enough to form continuous films and instead create island-like structures that are known to be strongly plasmonic.²²⁻²⁴ Figure 1b shows a high resolution transmission electron microscope (HRTEM) image of a Au nanoisland film with a nominal thickness of 5nm. Figure 1c shows the electric field intensity distribution of this Au nanoisland film calculated using the finite difference time domain (FDTD) method with a grid spacing of 2 Å.²⁵⁻²⁷ Small gaps between the nanoislands (~1-2 nm)

dominate the optical response of these films, which produce electric field intensity "hot spots", as shown in Figure 1c. In these localized hot spot regions, the electric field intensity can be as much as 1000 times larger than the incident electric field intensity resulting in SERS enhancement factors of 10⁶. ²⁵, ²⁸ Figure 1a shows a diagram illustrating the SERS-active electrode in which strips of 50 nm-thick Au are deposited on the left and right sides of the electrode, enabling electrical contact to be made to the film of Au nanoislands. Somewhat surprisingly, the plasmonic nanoislands are interconnected and provide an electrically continuous electrode with typical inplane resistances around 100-200 Ω . We have used these plasmon-resonant nanoislands for several years for SERS spectroscopy, plasmon-enhanced catalysis, and in FDTD studies of local field enhancement. ²⁸⁻⁴⁰ For the simulation, an HRTEM image of area 450nm × 300nm is used to define the spatial extent of Au nanoislands. A grid spacing of 2Å is used in the volume of 500nm × 500nm × 40nm around the film and 10nm elsewhere. A temporal grid spacing of 0.002 fsec is used with a total of 100,000-time steps. A planewave source is used, which irradiates the metal film with a Gaussian pulse with a spectrum of wavelengths ranging from 300nm to 800nm. Perfectly matched layers (PML) boundary conditions are used with 25 layers. The dielectric functions of Au are based on the optical constants given by Palik. We simulated the Au film using an X-polarized and a Ypolarized source In our previous work, Au nanoislands were deposited on top of monolayer graphene.⁴¹ In this configuration, the graphene provides additional electrical continuity between the metal nanoislands. However, we have found that the graphene reduces the SERS enhancement by ~10X and is not necessary to achieve electrical continuity within the electrode surface.

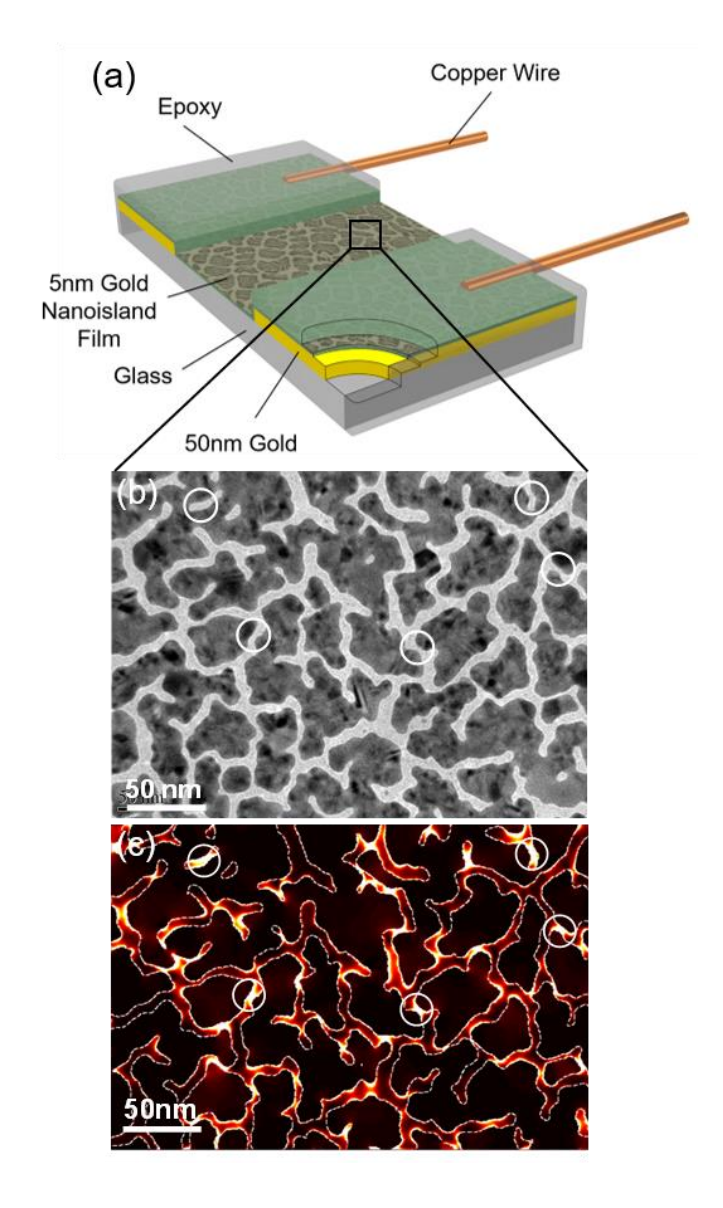


Figure 1. (a) Schematic diagram of the plasmon-resonant, SERS-active electrode fabricated with Au nanoislands. (b) TEM image and (c) FDTD simulations of the electric field distribution of the Au nanoisland film.

Figure 2a shows a schematic diagram illustrating the in situ Raman spectroscopy of these electrode surfaces under working electrochemical conditions using a water immersion lens (Leica model HC APO L #506155 40x, N.A. = 0.8). Here, the SERS-active electrode shown in Figure 1 serves as the working electrode with a Pt counter electrode (26 gauge, 99.9%) and Ag/AgCl reference electrode (BASI, MF-2052). A Gamry potentiostat (Reference 600+) is used to obtain cyclic voltammograms and apply various electrode potentials while Raman spectra are collected.

Raman spectra are collected using a 785nm wavelength laser (IPS, #32912) with a Renishaw in Via micro-Raman spectrometer. Raman spectra are collected for 1 minute of integration time with an incident laser power of 1.32 mW.

Ferrocene with a 6-carbon chain linker and thiol tether (i.e., 6-(ferrocenyl)hexanethiol, commercially available from Sigma Aldrich, #682527) is deposited on the Au nanoisland films, as illustrated in Figure 2b, using a 10 mM mixture in ethanol by soaking the substrate for 24 hours. Samples are rinsed in ethanol and then immersed into an aqueous solution of 0.1 M KCl for the measurements presented in Figure 3. Figure 2c shows a typical Raman spectrum of the ferrocene-functionalized, SERS-active electrode, which exhibits two sharp peaks corresponding to the C-H modes in the hexanethiol tail mode around 1072 cm⁻¹ and the C_P-breathing mode around 1104 cm⁻¹, illustrated in Figure 2d.⁴²

Figure 2d shows the calculated Raman spectra of 6-(ferrocenyl)hexanethiol using the NWChem program package. 43-45 The geometry optimizations and frequency calculations were carried out using the Becke, 3 parameter, Lee-Yang-Parr (B3LYP) exchange-correlation functional with dispersion correction (DFT-D3) by Grimme and the polarization-consistent (pc-1) basis. In Figure 2d, the predominant peaks are observed at 1069.79 cm⁻¹ and 1133.64 cm⁻¹, and correspond to the C_P-scissoring and breathing mode, respectively. These vibrational frequencies are slightly different from the corresponding frequencies observed experimentally (i.e., 1072 cm⁻¹ and 1104 cm⁻¹). Nevertheless, we observe good qualitative agreement between the calculated and measured spectra. Figure S2 of the Supplemental information shows a comparison of the eclipsed ferrocene and the 6-(ferrocenyl)hexanethiol plotted over the same wavenumber range. While the 6-(ferrocenyl)hexanethiol exhibits several additional peaks not seen in the eclipsed ferrocene, the

predominant peaks are observed at 1069.79 cm⁻¹ and 1133.64 cm⁻¹, and correspond to the C_P-scissoring and breathing mode, respectively.

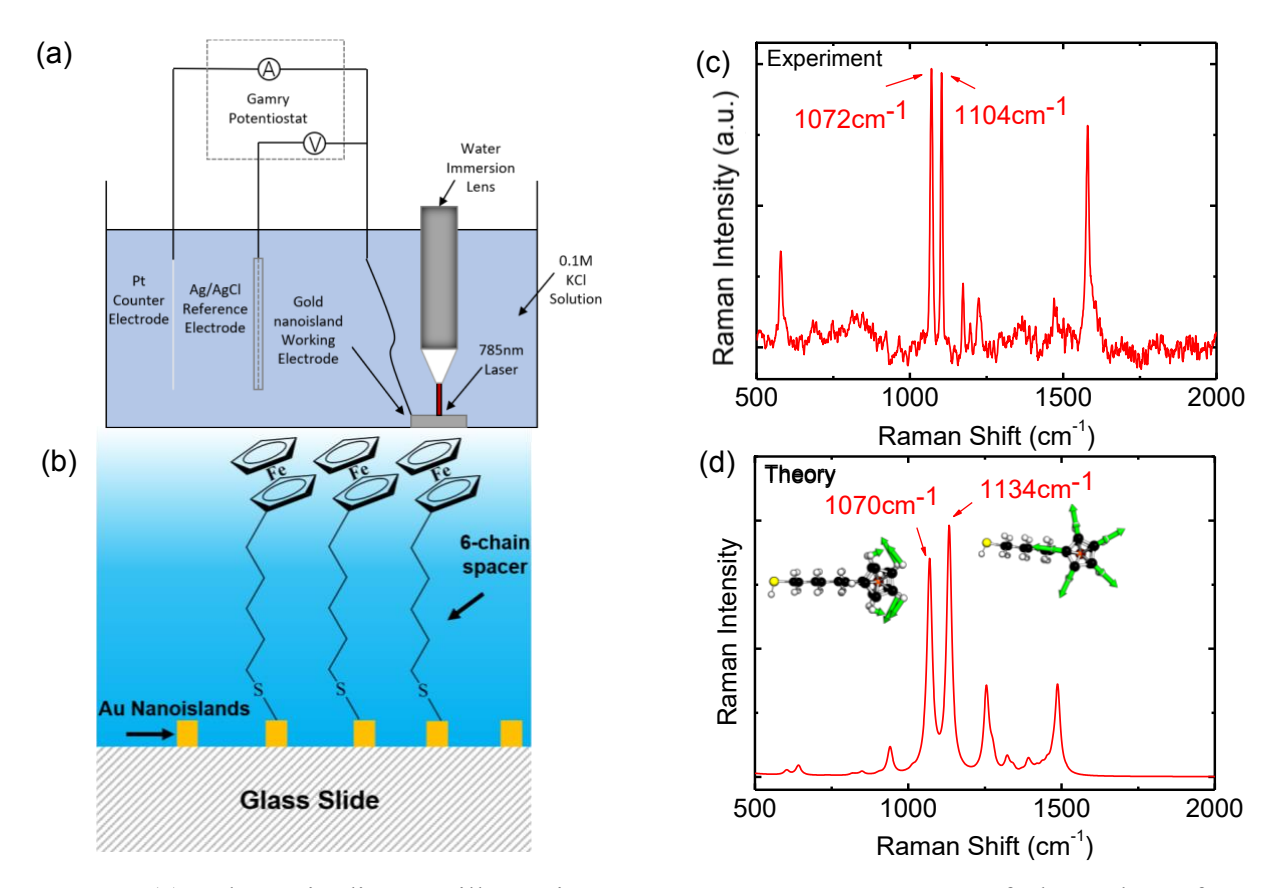


Figure 2. (a) Schematic diagram illustrating *in situ* Raman spectroscopy of electrode surfaces under working electrochemical conditions using a water immersion lens. (b) Cross-sectional diagram and (c) Raman spectrum of ferrocene-functionalized Au nanoisland substrate exhibiting sharp peaks corresponding to the C-H modes in the hexanethiol tail at 1072 cm⁻¹ and the C_P-breathing mode around 1104 cm⁻¹. (d) DFT calculated Raman spectrum of 6-(ferrocenyl)hexanethiol.

Figures 3a and 3b show the cyclic voltammograms taken of the ferrocene-functionalized, SERS-active electrode before and after the voltage-dependent Raman spectra plotted in Figures 3c and 3d. These CV curves, taken at various scan rates, exhibit clear peaks and dips corresponding to the oxidation of Fc to Fc⁺ and reduction of Fc⁺ to Fc, respectively. The redox potential of this reaction is taken as the midpoint between these peaks and dip and is approximately 0.4 V vs. Ag/AgCl. The Raman spectra plotted in Figures 3c and 3d show a clear voltage dependence that is repeatable after cycling the voltage several times. Here, we see the disappearance of the C_p-

breathing mode (1104 cm⁻¹) and a dramatic increase in the hexanethiol tail mode around (1072 cm⁻¹) over the applied voltage range. The peak near 1100 cm⁻¹ in cycle 2 is much weaker than in cycle 1 at 0V. However, the corresponding peak at 0.8V is quite reversible. Since the cycling of the voltage entails a bond rotation that may not be fully reversible. After three cycles, however, we found that there was substantial oxidation of the surface-bound Fc. We have also included additional datasets taken on a different sample, demonstrating the reproducibility of the measurements, as plotted in Figure S4 of the Supplemental Information document. Since our electrodes consist of a complex network of Au nanoislands, as shown in Figure 1, the finite series resistance between these nanoislands may contribute to the slow kinetics observed. Also, the compensating charge ions in solution can limit the charge transfer kinetics. Figure S6 shows C-V curves taken with a continuous 50 nm—thick Au electrode, demonstrating slightly improved kinetics, although no SERS spectra could be obtained from these continuous Au film electrodes.

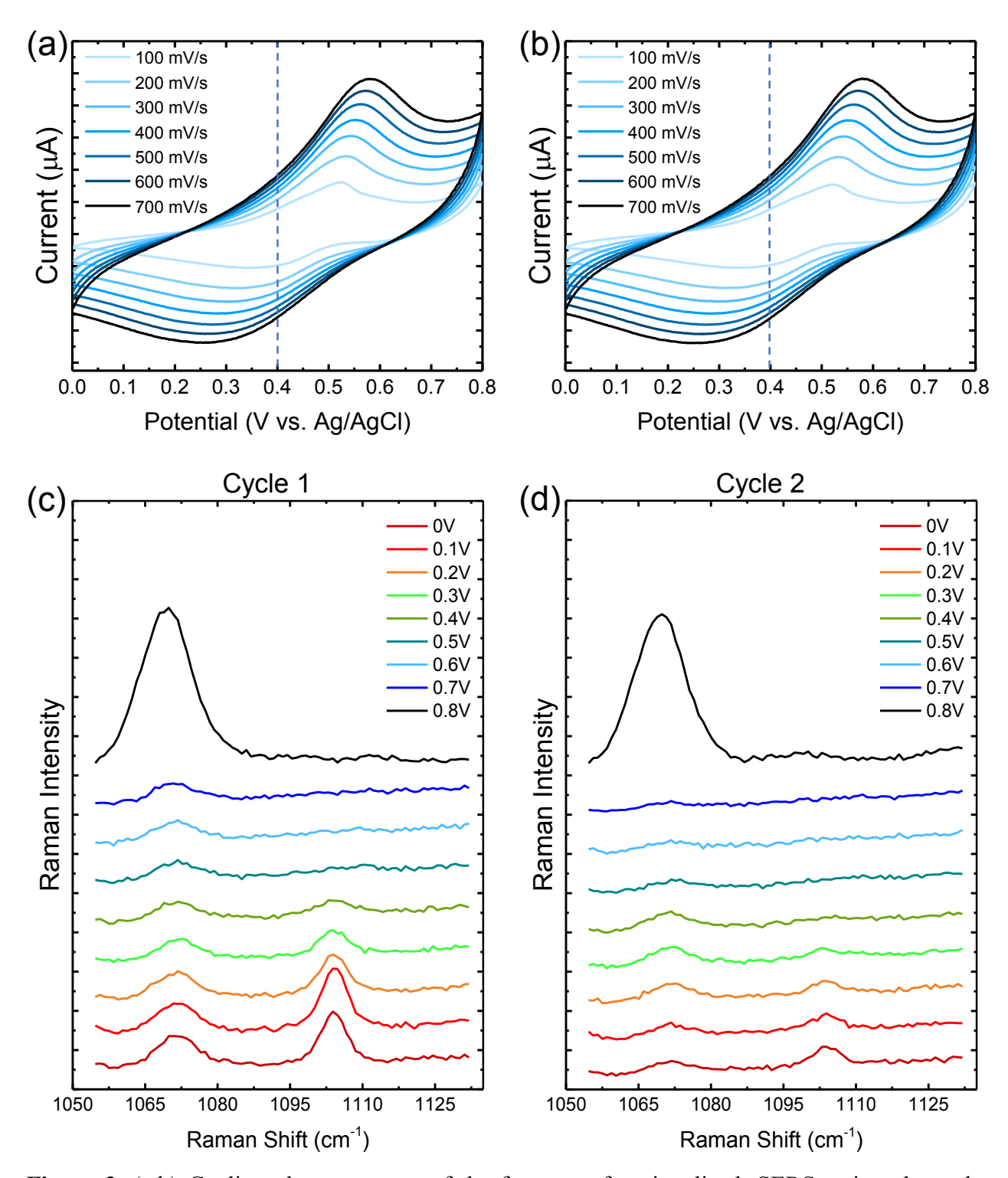


Figure 3. (a,b) Cyclic voltammograms of the ferrocene-functionalized, SERS-active electrode taken at various scan rates. (c,d) Raman spectra taken on the ferrocene-functionalized electrode under various applied electrode potentials vs. Ag/AgCl. This data is repeatable after cycling the voltage several times.

Figure 4 shows the calculated spectra of the 6-(ferrocenyl)hexanethiol (Fc) and 6-(ferrocenium)hexanethiol (Fc⁺). Due to the surface-selection rules in SERS we expect that the polarizability component aligned with the strong near field will dominate the SERS spectra. The surface-selection rules lead to a strong orientation dependence in the SERS spectra. To determine a good match between the simulated and experimental spectra we performed a search over the three principal angles: the tilt angle θ , axial rotation ϕ , and in-plane rotation χ (see diagram in Figure S1). Representative orientations are shown in Figure 4 with tilt angle θ , axial rotation ϕ , and in-plane rotation χ relative to the z-axis. Two major changes are seen in the spectra as the ferrocene is oxidized (i.e., $Fc \rightarrow Fc^+$): 1) the spectrum shifts from two peaks (for the Fc) to predominantly one peak (for Fc⁺) in the 1070 – 1140 cm⁻¹ range, and 2) the peak becomes centered around 1080 cm⁻¹ and increases by a factor of 10X in intensity in the Fc⁺ state. The physical mechanism corresponds to the coupling of the vibrations between the tail and the Fc⁺ group increasing in strength. Subsequently, the system begins to align itself along the z-axis as an indication of increased ordering. In addition, we measured Raman spectra of ferrocene (without the carbon chain linker and thiol tether), as plotted in Figure S5a of the Supplemental Information document. Figure S5b shows the DFT-calculated Raman spectrum of eclipsed ferrocene, which demonstrates good agreement with the experimentally measured spectrum. In the supporting information we also show that charging of the Fc⁺ is not sufficient to explain the observed changed in the SERS spectra.

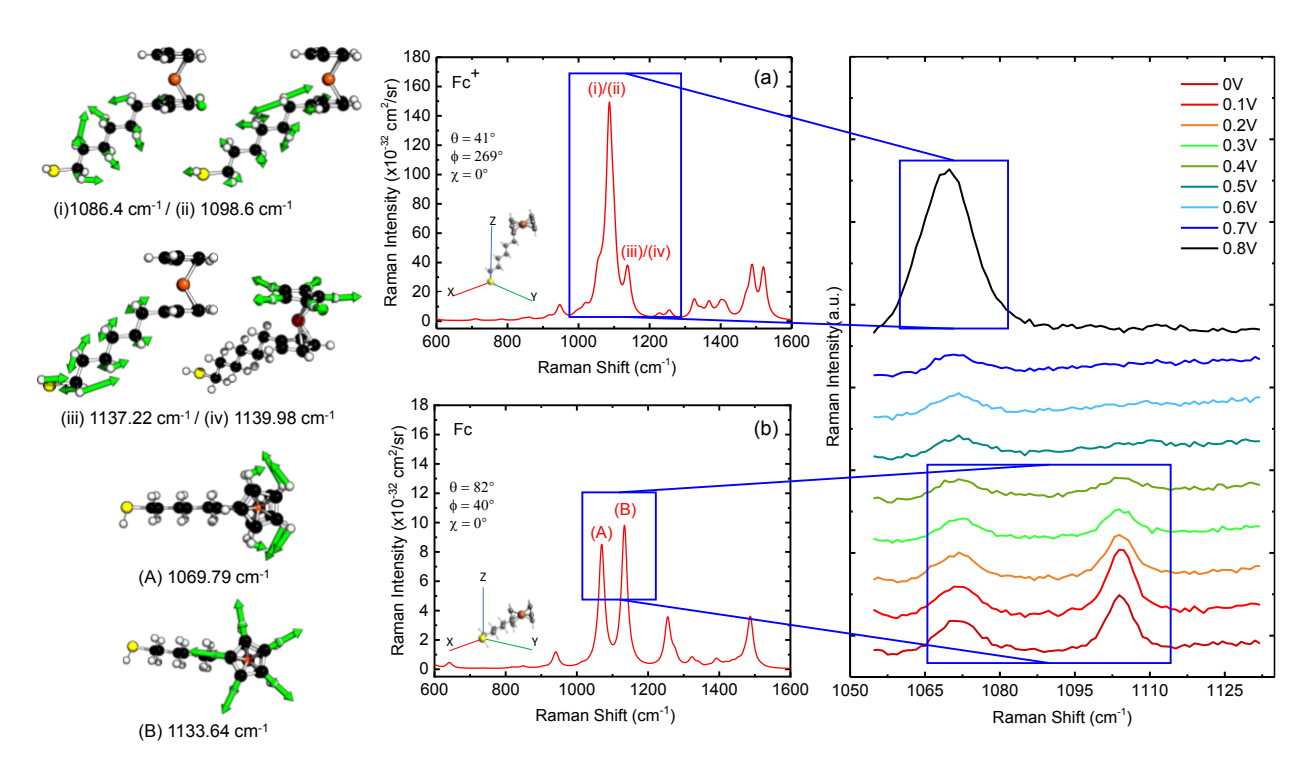


Figure 4. Calculated Raman spectra of (a) 6-(ferrocenium)hexanethiol and (b) 6-(ferrocenyl)hexanethiol.

As mentioned above, several previous studies using surface-enhanced infrared absorption spectroscopy (SEIRAS) have examined Fc-terminated electrodes as a function of electrode potential²⁰⁻²¹, which show a significant increase in the infrared absorption around 1100 cm⁻¹ due to the formation of a Fc⁺/anion complex. While this increase in the IR absorption stands in contrast to our observations, in which we see the disappearance of these two Raman peaks over the same range of applied electrochemical potentials, these spectra lend some insight into the changes observed in the present study. In addition to an increase in the intensity of the Fc-ring C-H stretching mode (around 1100 cm⁻¹) with increasing electrode potential, these SEIRAS studies observed a decrease in the intensity of two C-H stretching marker bands of the methylene groups, indicating that the angle between the alkyl chain and the normal to the electrode surface changes

upon oxidation/reduction of the Fc moieties. The latter observation confirms an orientation change (rotation) of the ferrocene moiety.

In conclusion, we have demonstrated a facile technique in which commercially available ferrocene molecules are deposited on a SERS-active Au electrode and used to detect charge transfer spectroscopically. The electrochemical oxidation of Fc to Fc⁺ results in a dramatic increase in the Raman intensity of the C-H mode in the hexanethiol tail and complete suppression of the C_p-breathing mode at high potentials. We also observe a redshift in the vibrational frequency of the hexanethiol tail mode corresponding to charge-induced rearrangement of the electronic and bonding structure of the molecule under electrochemical oxidation. This general approach opens up the possibility to study photo-initiated charge transfer and electrochemical potentials at semiconductor/liquid interfaces, as well as time-resolved Raman spectroscopy using pump-probe techniques. 49-50 Raman spectra calculated by density functional theory exhibits predominant peaks that agree well with our experimental observations. While the 6-(ferrocenyl)hexanethiol exhibits many additional peaks in the Raman spectra that are not seen in the eclipsed ferrocene, the predominant peaks are common to both molecules. The 1070 cm⁻¹ mode couples to the linker and is very sensitive to the orientation of the linker. As such, the $Fc \rightarrow Fc^+$ transition is associated with a slight change in the orientation, which gives rise to dramatic changes in the Raman spectra.

Acknowledgements

This research was supported by the U.S. Department of Energy, Office of Basic Energy Sciences award no. DESC0019322 (R.L.), the Army Research Office (ARO) award no. W911NF-22-1-0284 (Y.W.); National Science Foundation (NSF) award nos. CHE-2106151 (I.C. and L.J.), CHE-2106480 (S.W.), CBET-2012845 (Z.C.), and CBET-1954834 (I.A.); Air Force Office of Scientific Research (AFOSR) grant no. FA9550-19-1-0115 (B.Z.).

References

- 1. Maduraiveeran, G.; Jin, W., Nanomaterials based electrochemical sensor and biosensor platforms for environmental applications. *Trends in Environmental Analytical Chemistry* **2017**, *13*, 10-23.
- 2. Xiao, T.; Huang, J.; Wang, D.; Meng, T.; Yang, X., Au and Au-Based nanomaterials: Synthesis and recent progress in electrochemical sensor applications. *Talanta* **2020**, *206*, 120210.
- 3. Huang, Z.; Zhang, A.; Zhang, Q.; Cui, D., Nanomaterial-based SERS sensing technology for biomedical application. *Journal of Materials Chemistry B* **2019**, 7 (24), 3755-3774.
- 4. Yuan, Y.; Panwar, N.; Yap, S. H. K.; Wu, Q.; Zeng, S.; Xu, J.; Tjin, S. C.; Song, J.; Qu, J.; Yong, K.-T., SERS-based ultrasensitive sensing platform: An insight into design and practical applications. *Coordination Chemistry Reviews* **2017**, *337*, 1-33.
- 5. Moldovan, R.; Vereshchagina, E.; Milenko, K.; Iacob, B.-C.; Bodoki, A. E.; Falamas, A.; Tosa, N.; Muntean, C. M.; Farcău, C.; Bodoki, E., Review on combining surface-enhanced Raman spectroscopy and electrochemistry for analytical applications. *Analytica Chimica Acta* **2021**, 339250.
- 6. Hu, Y.; Wu, C.; Huang, S.; Luo, X.; Yuan, R.; Yang, X., A novel SERS substrate with high reusability for sensitive detection of miRNA 21. *Talanta* **2021**, *228*, 122240.
- 7. Tsai, M.-H.; Lin, Y.-K.; Luo, S.-C., Electrochemical SERS for in situ monitoring the redox states of PEDOT and its potential application in oxidant detection. *ACS applied materials & interfaces* **2018**, *11* (1), 1402-1410.
- 8. Choi, S.; Ahn, M.; Kim, J., Highly reproducible surface-enhanced Raman scattering-active Au nanostructures prepared by simple electrodeposition: Origin of surface-enhanced Raman scattering activity and applications as electrochemical substrates. *Analytica chimica acta* **2013**, 779, 1-7.
- 9. Wang, H. H.; Liu, C. Y.; Wu, S. B.; Liu, N. W.; Peng, C. Y.; Chan, T. H.; Hsu, C. F.; Wang, J. K.; Wang, Y. L., Highly raman-enhancing substrates based on silver nanoparticle arrays with tunable sub-10 nm gaps. *Advanced Materials* **2006**, *18* (4), 491-495.
- 10. Wilson, A. J.; Molina, N. Y.; Willets, K. A., Modification of the electrochemical properties of Nile Blue through covalent attachment to gold as revealed by electrochemistry and SERS. *The Journal of Physical Chemistry C* **2016**, *120* (37), 21091-21098.
- 11. Zaleski, S.; Cardinal, M. F.; Klingsporn, J. M.; Van Duyne, R. P., Observing single, heterogeneous, one-electron transfer reactions. *The Journal of Physical Chemistry C* **2015**, *119* (50), 28226-28234.
- 12. Gagne, R. R.; Koval, C. A.; Lisensky, G. C., Ferrocene as an Internal Standard for Electrochemical Measurements. *Inorg Chem* **1980**, *19* (9), 2854-2855.
- 13. Alehashem, S.; Chambers, F.; Strojek, J. W.; Swain, G. M.; Ramesham, R., Cyclic Voltammetric Studies of Charge-Transfer Reactions at Highly Boron-Doped Polycrystalline Diamond Thin-Film Electrodes. *Anal Chem* **1995**, *67* (17), 2812-2821.
- 14. Paul, A.; Borrelli, R.; Bouyanfif, H.; Gottis, S.; Sauvage, F., Tunable Redox Potential, Optical Properties, and Enhanced Stability of Modified Ferrocene-Based Complexes. *Acs Omega* **2019**, *4* (12), 14780-14789.
- 15. Smalley, J. F.; Feldberg, S. W.; Chidsey, C. E. D.; Linford, M. R.; Newton, M. D.; Liu, Y. P., The Kinetics of Electron-Transfer through Ferrocene-Terminated Alkanethiol Monolayers on Gold. *J Phys Chem-Us* **1995**, *99* (35), 13141-13149.

- 16. Choudhury, M. H.; Ciampi, S.; Lu, X. Y.; Kashi, M. B.; Zhao, C.; Gooding, J. J., Spatially confined electrochemical activity at a non-patterned semiconductor electrode. *Electrochim Acta* **2017**, *242*, 240-246.
- 17. Swearingen, C.; Wu, J.; Stucki, J.; Fitch, A., Use of ferrocenyl surfactants of varying chain lengths to study electron transfer reactions in native montmorillonite clay. *Environ Sci Technol* **2004**, *38* (21), 5598-603.
- 18. Inagaki, M.; Motobayashi, K.; Ikeda, K., Electrochemical THz-SERS Observation of Thiol Monolayers on Au(111) and (100) Using Nanoparticle-assisted Gap-Mode Plasmon Excitation. *The Journal of Physical Chemistry Letters* **2017**, *8* (17), 4236-4240.
- 19. Dendisová, M.; Havránek, L.; Ončák, M.; Matějka, P., In Situ SERS Study of Azobenzene Derivative Formation from 4-Aminobenzenethiol on Gold, Silver, and Copper Nanostructured Surfaces: What Is the Role of Applied Potential and Used Metal? *The Journal of Physical Chemistry C* **2013**, *117* (41), 21245-21253.
- 20. Rudnev, A. V.; Zhumaev, U.; Utsunomiya, T.; Fan, C. J.; Yokota, Y.; Fukui, K.; Wandlowski, T., Ferrocene-terminated alkanethiol self-assembled monolayers: An electrochemical and in situ surface-enhanced infra-red absorption spectroscopy study. *Electrochim Acta* **2013**, *107*, 33-44.
- 21. Tu, K. Y.; Morhart, T. A.; Read, S. T.; Rosendahl, S. M.; Burgess, I. J., Probing Heterogeneity in Attenuated Total Reflection Surface-Enhanced Infrared Absorption Spectroscopy (ATR-SEIRAS) Response with Synchrotron Infrared Microspectroscopy. *Appl Spectrosc* **2021**, *75* (9), 1198-1206.
- 22. Kumar, R.; Zhou, H.; Cronin, S. B., Surface-enhanced Raman spectroscopy and correlated scanning electron microscopy of individual carbon nanotubes. *Applied Physics Letters* **2007**, *91*, 223105.
- 23. Kneipp, K.; Kneipp, H.; Corio, P.; Brown, S. D. M.; Shafer, K.; Motz, J.; Perelman, L. T.; Hanlon, E. B.; Marucci, A.; Dresselhaus, G.; Dresselhaus, M. S., Surface-enhanced and normal Stokes and anti-Stokes Raman spectroscopy of single-walled carbon nanotubes. *Physical Review Letters* **2000**, *84* (15), 3470-3473.
- 24. Liu, Z.; Hou, W.; Pavaskar, P.; Aykol, M.; Cronin, S., Plasmon Resonant Enhancement of Photocatalytic Water Splitting Under Visible Illumination. *Nano Letters* **2011**, *11*, 1111.
- 25. Pavaskar, P.; Theiss, J.; Cronin, S. B., Plasmonic hot spots: nanogap enhancement vs. focusing effects from surrounding nanoparticles. *Optics Express* **2012**, *20* (13), 14656-14662.
- 26. Pavaskar, P.; Hsu, I. K.; Theiss, J.; Hsuan Hung, W.; Cronin, S. B., A microscopic study of strongly plasmonic Au and Ag island thin films. *Journal of Applied Physics* **2013**, *113* (3).
- 27. Pavaskar, P.; Cronin, S. B., Iterative optimization of plasmon resonant nanostructures. *Applied Physics Letters* **2009**, *94* (25).
- 28. Pavaskar, P.; Hsu, I. K.; Theiss, J.; Hung, W. H.; Cronin, S. B., A microscopic study of strongly plasmonic Au and Ag island thin films. *Journal of Applied Physics* **2013**, *113* (3).
- 29. Chen, J.; Bailey, C. S.; Hong, Y.; Wang, L.; Cai, Z.; Shen, L.; Hou, B.; Wang, Y.; Shi, H.; Sambur, J.; Ren, W.; Pop, E.; Cronin, S. B., Plasmon-Resonant Enhancement of Photocatalysis on Monolayer WSe2. *ACS Photonics* **2019**, *6* (3), 787-792.
- 30. Hao, E.; Schatz, G. C., Electromagnetic fields around silver nanoparticles and dimers. *J Chem Phys* **2004**, *120* (1), 357-66.
- 31. Hou, W.; Cronin, S. B., A Review of Surface Plasmon Resonance-Enhanced Photocatalysis. *Advanced Functional Materials* **2013**, *23* (13), 1612-1619.

- 32. Hou, W.; Hung, W. H.; Pavaskar, P.; Goeppert, A.; Aykol, M.; Cronin, S. B., Photocatalytic Conversion of CO2 to Hydrocarbon Fuels via Plasmon-Enhanced Absorption and Metallic Interband Transitions. *ACS Catalysis* **2011**, *I* (8), 929-936.
- 33. Hou, W.; Liu, Z.; Pavaskar, P.; Hung, W. H.; Cronin, S. B., Plasmonic enhancement of photocatalytic decomposition of methyl orange under visible light. *Journal of Catalysis* **2011**, 277 (2), 149-153.
- 34. Hou, W.; Pavaskar, P.; Liu, Z.; Theiss, J.; Aykol, M.; Cronin, S. B., Plasmon resonant enhancement of dye sensitized solar cells. *Energy & Environmental Science* **2011**, *4* (11).
- 35. Hung, W. H.; Aykol, M.; Valley, D.; Hou, W.; Cronin, S. B., Plasmon resonant enhancement of carbon monoxide catalysis. *Nano Lett* **2010**, *10* (4), 1314-8.
- 36. Hung, W. H.; Hsu, I. K.; Bushmaker, A.; Kumar, R.; Theiss, J.; Cronin, S. B., Laser directed growth of carbon-based nanostructures by plasmon resonant chemical vapor deposition. *Nano Lett* **2008**, *8* (10), 3278-82.
- 37. Lin, J. J.; Shen, J. X.; Wang, R. J.; Cui, J. J.; Zhou, W. J.; Hu, P. G.; Liu, D. O.; Liu, H.; Wang, J. Y.; Boughton, R. I.; Yue, Y. Z., Nano-p-n junctions on surface-coarsened TiO₂ nanobelts with enhanced photocatalytic activity. *J. Mater. Chem.* **2011**, *21* (13), 5106-5113.
- 38. Pavaskar, P.; Theiss, J.; Cronin, S. B., Plasmonic hot spots: nanogap enhancement vs. focusing effects from surrounding nanoparticles. *Opt Express* **2012**, *20* (13), 14656-62.
- 39. Qiu, J.; Zeng, G.; Pavaskar, P.; Li, Z.; Cronin, S. B., Plasmon-enhanced water splitting on TiO2-passivated GaP photocatalysts. *Physical Chemistry Chemical Physics* **2014**, *16* (7), 3115-3121.
- 40. Li, S.; Zhao, B.; Aguirre, A.; Wang, Y.; Li, R.; Yang, S.; Aravind, I.; Cai, Z.; Chen, R.; Jensen, L.; Cronin, S. B., Monitoring Reaction Intermediates in Plasma-Driven SO2, NO, and NO2 Remediation Chemistry Using In Situ SERS Spectroscopy. *Anal Chem* **2021**, *93* (16), 6421-6427.
- 41. Shi, H.; Cai, Z.; Patrow, J.; Zhao, B.; Wang, Y.; Wang, Y.; Benderskii, A.; Dawlaty, J.; Cronin, S. B., Monitoring Local Electric Fields at Electrode Surfaces Using Surface Enhanced Raman Scattering-Based Stark-Shift Spectroscopy during Hydrogen Evolution Reactions. *ACS Applied Materials & Interfaces* **2018**, *10* (39), 33678-33683.
- 42. Shimei, J.; Yue, W., Vibrational spectra of an open ferrocene and a half-open ferrocene. *Spectrochim Acta A* **1999**, *55* (5), 1025-1033.
- 43. te Velde, G.; Bickelhaupt, F. M.; Baerends, E. J.; Guerra, C. F.; Van Gisbergen, S. J. A.; Snijders, J. G.; Ziegler, T., Chemistry with ADF. *J Comput Chem* **2001**, *22* (9), 931-967.
- 44. Fonseca Guerra, C.; Snijders, J. G.; te Velde, G.; Baerends, E. J., Towards an order-N DFT method. *Theoretical Chemistry Accounts* **1998**, *99* (6), 391-403.
- 45. Baerends, E. J., et al., ADF. *Theoretical Chemistry, Vrije Universiteit: Amsterdam, The Netherlands*, **2019**.
- 46. Becke, A. D., Density-Functional Exchange-Energy Approximation with Correct Asymptotic-Behavior. *Phys Rev A* **1988**, *38* (6), 3098-3100.
- 47. Perdew, J. P., Density-Functional Approximation for the Correlation-Energy of the Inhomogeneous Electron-Gas. *Phys Rev B* **1986**, *33* (12), 8822-8824.
- 48. Grimme, S.; Ehrlich, S.; Goerigk, L., Effect of the Damping Function in Dispersion Corrected Density Functional Theory. *J Comput Chem* **2011**, *32* (7), 1456-1465.
- 49. Frontiera, R. R.; Mathies, R. A., Femtosecond stimulated Raman spectroscopy. *Laser & Photonics Reviews* **2011**, *5* (1), 102-113.

50. Frontiera, R. R.; Henry, A. I.; Gruenke, N. L.; Van Duyne, R. P., Surface-Enhanced Femtosecond Stimulated Raman Spectroscopy. *Journal of Physical Chemistry Letters* **2011**, *2* (10), 1199-1203.